

Research Article

Comparative Molecular Mechanistic Modelling of a Tubular Thermal Cracker in Two and Three Dimensions

B.A. Olufemi and O.O. Famuyide

Department of Chemical Engineering, University of Lagos, Akoka, Lagos, Nigeria

Abstract: This study aimed at the modelling of a tubular thermal cracker in two and three dimensions using 0.15 kg/h of ethane and 1.5 kg/h of nitrogen in laminar flow using a molecular mechanistic model for ethane cracking, followed by the solution and comparison of the results obtained. This was used to find the effect that spatial development had on the generated profiles. The purpose was achieved by deriving the requisite model equations from mass, energy and momentum balances consisting of nine coupled partial differential equations for each of the spatial considerations and using the finite difference numerical scheme to solve. Throughout the reactor length of 1.20 m and radius of 0.0125 m, the resulting concentration and temperature profiles were predicted. In comparison, the profiles from the two and three dimensional developments showed that even though angular variations are small in the three dimensional approach, they are still present and their consideration could be helpful in the design of tubular thermal crackers.

Keywords: Finite difference, modelling, partial differential equations, Three Dimensional (3-D), tubular thermal cracker, Two Dimensional (2-D)

INTRODUCTION

By definition, cracking refers to breaking of higher boiling petroleum fractions into lower boiling lighter fractions. It is considered an endothermic reaction. There is heat supply to the parent compound (s) until they ignite and are converted to various products depending on the nature of the parent compound, cracking temperature and the type of cracking employed (Walter *et al.*, 1988). Thermal cracking is carried out in tubular reactor system with the supply of heat externally. The tubular reactor is a conduit suitable for reactants flow with no attempt made to increase the natural degree of mixing (Rutherford, 1989).

Since the heat transfer within a tube is not instantaneous, the endothermic reaction gives rise to problems of temperature control and maintenance, as well as selectivity which are very difficult to solve. The furnace caters for the heat requirements, radiative heat transfer heats up the tube walls and heat is further conveyed to the reaction mass from the heated tube walls. The transport of heat in the tube is responsible for the variation in reaction rates in radial, axial and angular directions depending on manner of heating employed, which result in gradients being setup in these directions. Olefins production from natural gas has been reported by Holman *et al.* (1995) in addition to the conventional feeds being used.

In thermal cracking, some modelling studies are available in the literature like Behloulav *et al.* (2003) and Niaei *et al.* (2004). Some are based on the plug flow assumptions which are 1-dimensional model where the lateral gradients are considered negligible. As reported, Sundaram and Froment (1979) have compared the predictions of a 1-dimensional model to a 2-dimensional model for a single irreversible reaction. The 2-dimensional model seems to give better predictions. A fast operating algorithm for thermal cracking furnaces had been proposed by Xu *et al.* (2002), for optimization of the steam crackers, which again is based upon plug flow conditions. In addition, Sundaram and Froment (1979) have compared the one-dimensional model to a two dimensional model for a pipe reactor with a single molecular reaction using the laminar and turbulent flow regimes. It was observed by Sundaram and Froment (1979) that a typical radial concentration and temperature profile exists. As they observed also, the one-dimensional model gives better predictions, if an averaged *Nusselt* number from a two-dimensional model is incorporated into the one-dimensional model. In another study by Sundaram and Froment (1980), these findings have been reported to hold for 2-dimensional modelling of ethane thermal cracker for turbulent conditions. Garg and Srivastava (2006) had also reported a 2-dimensional modelling for tubular thermal cracking of ethane.

Corresponding Author: B.A. Olufemi, Department of Chemical Engineering, University of Lagos, Akoka, Lagos, Nigeria, Tel: +234-802-316-2183

This work is licensed under a Creative Commons Attribution 4.0 International License (URL: <http://creativecommons.org/licenses/by/4.0/>).

It had been proposed that the resistance in the radial direction to heat and mass transfer controls the extent of reaction and product distribution obtained from the reactor. Garg and Srivastava (2001) found that annular reactors have a distinct advantage of lower diffusion path over the tubular reactors, which also lowers the radial resistance. This also implies higher surface area which can be utilized for better heat transfer. Earlier, the radial diffusional mass transfer in a fully developed laminar flow through an annular cylindrical reactor for a first order heterogeneous reaction at the wall had been studied (Houzelot and Villiermaux, 1977).

The three dimensional model seems to explain reaction systems in which non-circumferential heating is utilized. The reactor is usually a differential sized tubular conduit, upon which modelling is based using the equations of mass, energy and momentum balance. A molecular mechanistic reactions scheme for ethane cracking is usually adapted from Froment and Bischoff (1990). The 2 and 3 dimensional model from this reaction scheme seems suitable for predicting feed and products concentration as well as temperature profiles in radial, axial and angular (for 3-D) directions.

This present study is intended as an inquisitive effort for the three-dimensional modelling of a tubular thermal cracker which seems to be a largely unexplored area. Ethane was used in the development of this present study as the cracking reaction of heavier compounds involves numerous steps which increase the complexity of the resulting reactions.

METHODOLOGY

Model development: The development of these models made some inextricable assumptions without which the analyses would be profoundly complex. These assumptions are chosen to simplify the resulting PDEs within reasonable limits while avoiding over-simplification so that the whole purpose of the modelling and simulation will not be lost. The proposed model for ethane cracking in the tubular reactor is based upon the following assumptions:

- The reactor operates under steady state conditions because the reactor has continuous flow that stabilizes and gives rise to steady state condition.
- The flow regime is laminar due to its similarity to a laboratory scale reactor.
- The wall temperature is high and constant because heat is required for the system from the outside (endothermicity of system).

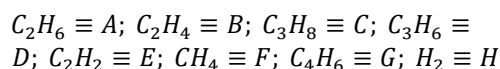
Table 1: Molecular reaction scheme and kinetic parameters for the thermal cracking of ethane as obtained from Froment and Bischoff (1990)

Reaction	Order	A_0 (s^{-1})	E (kJ/mol)
1) $C_2H_6 \xrightarrow{k_1} C_2H_4 + H_2$	1	4.65×10^{13}	273,020
2) $C_2H_4 + H_2 \xrightarrow{k_2} C_2H_6$	2	8.75×10^{8a}	136,870
3) $2C_2H_6 \xrightarrow{k_3} C_3H_8 + CH_4$	1	3.85×10^{11}	273,190
4) $C_3H_8 \xrightarrow{k_4} C_2H_2 + CH_4$	1	9.81×10^8	154,580
5) $C_2H_2 + CH_4 \xrightarrow{k_5} C_3H_6$	2	5.87×10^{4a}	29,480
6) $C_2H_2 + C_2H_4 \xrightarrow{k_6} C_4H_6$	2	1.03×10^{12a}	172,750
7) $C_2H_4 + C_2H_6 \xrightarrow{k_7} C_3H_6 + CH_4$	2	7.08×10^{13a}	253,010

^a: In units of s^{-1} or $m^3/kmol.s$

Other needed assumptions are made as they come up in the course of the model developments. The molecular scheme used here is presented in the Table 1, also shown are the kinetic parameters that accompany each reaction. Froment and Bischoff (1990) and Garg *et al.* (2006) have used similar schemes.

The reactions shown in Table 1 involve eight species in seven reactions; two of the reactions are reversible which make for five reactions in effect. The following designations are used all through the study:



The reaction rates for the species are:

$$r_A = -k_1 C_A + k_2 C_B C_H - k_3 C_A - k_7 C_B C_A \quad (1)$$

$$r_B = k_1 C_A - k_2 C_B C_H - k_6 C_B C_E - k_7 C_B C_A \quad (2)$$

$$r_C = k_3 C_A \quad (3)$$

$$r_D = k_7 C_B C_A - k_4 C_D + k_5 C_E C_F \quad (4)$$

$$r_E = k_4 C_D - k_5 C_E C_F - k_6 C_B C_E \quad (5)$$

$$r_F = k_3 C_A + k_4 C_D - k_5 C_E C_F + k_7 C_B C_A \quad (6)$$

$$r_G = k_6 C_B C_E \quad (7)$$

$$r_H = k_1 C_A - k_2 C_B C_H \quad (8)$$

where the rate constants are expressible as:

$$k_i = A_{oi} e^{-\frac{E_i}{RT}}; T [=] K \quad (9)$$

and linearized by a truncated Taylor's Series of the form:

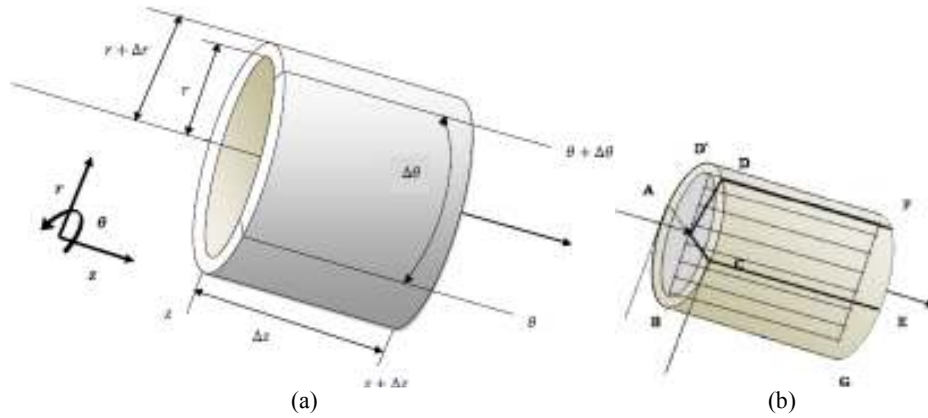


Fig. 1: (a) 3-dimensional tubular model, (b) mesh generation

$$k(T) = k(T_0) + \left. \frac{dk}{dT} \right|_{T=T_0} (T - T_0)$$

$$\Rightarrow k(T) = k(873.16) + (T - 873.16) \left. \frac{dk}{dT} \right|_{T=873.16} \quad (10)$$

A mass balance is written for each specie and a heat balance for the overall system.

The two-dimensional model equations: Derivations here are based on a cylindrical shell of dimensions Δr and Δz at a distance z from the entrance and a distance r from the centre.

The generated mass balance for the i th specie is:

$$D_i \frac{\partial^2 C_i}{\partial r^2} + \frac{1}{r} D_i \frac{\partial C_i}{\partial r} - U_z \frac{\partial C_i}{\partial z} + r_i = 0 \quad (11)$$

where,

$$i = A, B, C, D, E, F, G, H$$

and the simplified energy balance:

$$\frac{k_e}{r} \frac{\partial T}{\partial r} + k_e \frac{\partial^2 T}{\partial r^2} + k_e \frac{\partial^2 T}{\partial z^2} - U_z C_{pm} \frac{\partial T}{\partial z} + \Delta H_{rxn} r_i = 0 \quad (12)$$

The velocity profile is:

$$v_z = \frac{\epsilon_r R^2}{4 \mu} \left(1 - \left(\frac{r}{R} \right)^2 \right) \quad (13)$$

The boundary conditions are as follows:

$$\text{Inlet}(z = 0): C_i(r, 0) = C_{i0}; T(r, 0) = T_0$$

$$\text{Wall}(r = R): \frac{\partial C_i}{\partial r} = 0; T = T_w$$

$$\text{Centre}(r = 0): \frac{\partial C_i}{\partial r} = 0; \frac{\partial T}{\partial r} = 0$$

$$\text{Outlet}(z = L): \frac{\partial C_i}{\partial z} = 0; \frac{\partial T}{\partial z} = 0 \quad (14)$$

The three-dimensional model equations: For this development a shell of dimensions $\Delta r, \Delta z$ and $\Delta \theta$ is used. The mass balance and energy balance are respectively:

$$D_e \frac{\partial^2 C_i}{\partial r^2} + \frac{1}{r} D_i \frac{\partial C_i}{\partial r} + \frac{1}{r} D_i \frac{\partial^2 C_i}{\partial \theta^2} + D_i \frac{\partial^2 C_i}{\partial z^2} - U_z \frac{\partial C_i}{\partial z} + r_i = 0 \quad (15)$$

and,

$$k_e \frac{\partial^2 T}{\partial r^2} + \frac{1}{r} k_e \frac{\partial T}{\partial r} + \frac{1}{r} k_e \frac{\partial^2 T}{\partial \theta^2} + k_e \frac{\partial^2 T}{\partial z^2} - U_z C_{pm} \frac{\partial T}{\partial z} + \Delta H_{rxn} \cdot r_i = 0 \quad (16)$$

For a completeness of procedure the velocity profile in 3-D is:

$$-\frac{1}{r} \frac{\partial \left(r \left(-\mu \frac{dv_z}{dr} \right) \right)}{\partial r} + \frac{1}{r} \frac{\partial \left(-\mu \frac{dv_z}{d\theta} \right)}{\partial \theta} + \frac{\partial P_z}{\partial z} + \rho g \sin \theta = 0 \quad (17)$$

In order to create a basis for the three-dimensional developments, it is presupposed that, as opposed to the case for two-dimensions, non-circumferential heating is employed for the thermal cracker under review here which induces specie and reactor property gradations in the axial, radial and angular directions. The boundary conditions for this case are chosen bearing in mind that only one side (Fig. 1) of the reactor is at 950°C; the other diametrically opposite half only receives heat from the high temperature side. This scenario may be obtained in situations where a side of the cracker tube is inaccessible so that only the exposed and reachable part can be heated.

As a result of the foregoing explanations, the mesh for the 3D Profile covers the entire Diameter (BGFD) of the tubular reactor. The mesh for the angular variations covers only a quarter of the reactor surface

(CEFD) on the low temperature side since the properties of the other quarter is only a repetition of that of the first due to their symmetry. Axial variations still occur down the reactor axis.

From Fig. 1 the following boundary conditions were obtained:

$$\text{Inlet } (z = 0): C_i(r, 0) = C_{i0}; T(r, 0) = T_0$$

$$\text{At the Wall (B)}: \frac{\partial C_i}{\partial r} = 0; T = T_w$$

$$\text{At the Wall (D')}: \frac{\partial C_i}{\partial r} = 0; \frac{\partial T}{\partial r} = 0$$

$$\text{At the Wall (C)}: \frac{\partial C_i}{\partial \theta} = 0; T = T_w$$

$$\text{At the Wall (D)}: \frac{\partial C_i}{\partial \theta} = 0; \frac{\partial T}{\partial \theta} = 0$$

$$\text{Outlet } (z = L): \frac{\partial C_i}{\partial z} = 0; \frac{\partial T}{\partial z} = 0 \quad (18)$$

Requisite data:

Length of tubular cracker, $L = 1.20 \text{ m}$

Radius of cracking tubes, $r = 0.0125 \text{ m}$

Mass flow rate of feed
 = 0.15 kg/hr ethane
 + 1.5 kg/hr nitrogen Molar ethane feed rate, F_{A_0}
 = $1.39 \times 10^{-6} \text{ kmol/s}$

Concentration of feed ethane, $C_{A_0} =$
 $1.07 \text{ gmol/m}^3 = 1.07 \times 10^{-3} \text{ kmol/m}^3$

Feed temperature, $T_0 = 600^\circ\text{C} = 873.16\text{K}$

Reactor wall temperature = $950^\circ\text{C} = 1223.16\text{K}$

Diffusivity values, enthalpies of formation and heat capacity values are sourced from Perry and Chilton (1997), Himmeblau (1989) and Garg *et al.* (2006).

NUMERICAL SCHEME

The PDEs expressed in Eq. (11), (12), (14) and (15) are discretized using the finite difference implicit scheme. This is done by substituting each of the differential term in the PDEs with a finite difference expression corresponding to the order of the differential term.

For the 2-D development, the axial and radial dimensions were both divided into 10 sections, creating a mesh with 40 boundary nodal points and 81 interior mesh points:

$$h_r = \frac{0.0125}{10} = 0.00125\text{m} \text{ and } h_z = \frac{1.2}{10} = 0.12\text{m}$$

On solving Eq. (11) for each of the species and (12) alongside their respective boundary conditions the concentration and temperature profiles are generated. The discretized 2-D model equations were obtained as:

$$\left(\frac{D_i}{h_r^2} + \frac{D_i}{2rh_r}\right)C_{J,I+1} + \left(-2\frac{D_i}{h_r^2} - \frac{U_z}{h_z}\right)C_{J,I} + \left(\frac{D_i}{h_r^2} - \frac{D_i}{2rh_r}\right)C_{J,I-1} + \left(\frac{U_z}{h_z}\right)C_{J-1,I} + r_i = 0 \quad (19)$$

and,

$$\left(\frac{k_e}{2rh_r} + \frac{k_e}{h_r^2}\right)T_{J,I+1} + \left(-2\frac{k_e}{h_r^2} - 2\frac{k_e}{h_z^2} - \frac{U_z C_{pm}}{h_z}\right)T_{J,I} + \left(\frac{k_e}{h_r^2} - \frac{k_e}{2rh_r}\right)T_{J,I-1} + \left(\frac{k_e}{h_z^2}\right)T_{J+1,I} + \left(\frac{k_e}{h_z^2} + \frac{U_z C_{pm}}{h_z}\right)T_{J-1,I} + \Sigma(\Delta H_{R_x})r_i = 0 \quad (20)$$

$$\text{Inlet. } I = 1 \dots M, J = 1 : C_{A\ 1,I} = C_{A0}, C_{B\ 1,I} = C_{C\ 1,I} = \dots = C_{H\ 1,I} = 0; T_{1,I} = T_0$$

At the wall. $I = 1 \dots M, J = 1$:

$$\frac{C_{J,I} - C_{J,I-1}}{h_r} = 0; T = T_w = 1223.16\text{K}$$

Centre(symmetry)line. $I = 1, J = 1 \dots N$:

$$\frac{C_{J,I+1} - C_{J,I}}{h_r} = 0; \frac{T_{J,I+1} - T_{J,I}}{h_r} = 0$$

Outlet($z = L = \text{length}$). $I = 1 \dots M, J = N$:

$$\frac{C_{J,I} - C_{J-1,I}}{h_z} = 0; \frac{T_{J,I} - T_{J-1,I}}{h_z} = 0 \quad (21)$$

In the 3-D scenario, the axial, angular and radial dimensions were each divided into 10 sections, creating a mesh with 62 boundary nodal points and 162 interior mesh points:

$$h_r = \frac{0.025}{10} = 0.0025\text{m}; h_\theta = \frac{\pi/2}{10} = 0.1571^\circ \text{ and } h_z = \frac{1.2}{10} = 0.12\text{m}$$

The desired profiles were then developed from the discretized 3D model equations and their respective boundary conditions:

$$\begin{aligned} & \left(\frac{D_i}{h_r^2} + \frac{D_i}{2rh_r} \right) C_{J,I+1,K} + \left(-2 \frac{D_i}{h_r^2} - \frac{U_z}{h_z} - 2 \frac{D_i}{rh_\theta^2} \right) \\ & C_{J,I,K} + \left(\frac{D_i}{h_r^2} - \frac{D_i}{2rh_r} \right) C_{J,I-1,K} + \left(\frac{U_z}{h_z} \right) C_{J-1,I,K} \\ & + \left(\frac{D_i}{rh_\theta^2} \right) C_{J,I,K+1} + \left(\frac{D_i}{rh_\theta^2} \right) C_{J,I,K-1} + r_i = 0 \quad (22) \end{aligned}$$

and,

$$\begin{aligned} & \left(\frac{k_e}{2rh_r} + \frac{k_e}{h_r^2} \right) T_{J,I+1,K} + \left(-2 \frac{k_e}{h_r^2} - 2 \frac{k_e}{h_z^2} - \frac{U_z C_{pm}}{h_z} - \right. \\ & \left. 2k_e h_\theta^2 T_{J,I,K} + k_e h_r^2 - k_e 2rh_r T_{J,I-1,K} \right. \\ & + \left(\frac{k_e}{h_z^2} \right) T_{J+1,I,K} + \left(\frac{k_e}{h_z^2} + \frac{U_z C_{pm}}{h_z} \right) T_{J-1,I,K} + \\ & \left(\frac{k_e}{rh_\theta^2} \right) T_{J,I,K+1} + \left(\frac{k_e}{rh_\theta^2} \right) T_{J,I,K-1} \\ & + \sum (\Delta H_{R_x}) r_i = 0 \quad (23) \end{aligned}$$

$$\text{Inlet. } I = 1..M, J = 1, K = 1 \dots O$$

$$C_{A \ 1,I,K} = C_{A_0}$$

$$C_{B \ 1,I,K} = C_{C \ 1,I,K} = \dots = C_{H \ 1,I,K} = 0$$

$$T_{1,I,K} = T_0 = 873.16K$$

$$\text{At the wall(B) } I = 1, J = 1 \dots N, K = 1 \dots O:$$

$$\frac{C_{J,I,K} - C_{J,I-1,K}}{h_r} = 0; T = T_w = 1223.16K$$

$$\text{At the wall(D')} I = M, J = 1 \dots N, K = 1 \dots O:$$

$$\frac{C_{J,I,K} - C_{J,I-1,K}}{h_r} = 0; \frac{T_{J,I,K} - T_{J,I-1,K}}{h_r} = 0$$

$$\text{At the wall(C) } I = 1 \dots 0.5M, J = N, K = 1, \dots O:$$

$$\frac{C_{J,I,K} - C_{J,I,K-1}}{h_\theta} = 0; T = T_w = 1223.16K$$

$$\text{At the wall(D) } I = 1 \dots M, J = N, K = 1 \dots O:$$

$$\frac{C_{J,I,K} - C_{J,I,K-1}}{h_\theta} = 0; \frac{T_{J,I,K} - T_{J,I,K-1}}{h_\theta} = 0$$

$$\text{Outlet}(z = L). I = 1 \dots M, J = N, K = 1 \dots O:$$

$$\frac{C_{J,I,K} - C_{J-1,I,K}}{h_z} = 0; \frac{T_{J,I,K} - T_{J-1,I,K}}{h_z} = 0$$

The equations involving concentration can be written for each of the eight species. Each of these sets of equations for each species as well as the set for temperatures, written for a given axial position can be represented in the matrix form:

$$A \cdot X = B$$

The equations are first discretized using the finite difference implicit scheme before being solved by choosing an appropriate grid size (equal grid numbers on both axes in this case) and employing the Gauss-Seidel Algorithm in MATLAB®.

RESULTS AND DISCUSSION

The model equations are discretized with the finite difference numerical scheme and solved a pair at a time, i.e., a concentration model expression for a particular specie alongside the temperature model equation written for the same specie; the profile development was done this way because the model equations; concentration, temperature and velocity present a case of strong coupling. The generated temperature profile from the solution of any pair of equations was employed in simplifying all subsequent solutions since one and only one temperature profile exists through the tubular thermal cracker by the operation.

The profiles are generated by breaking the composite difference equation into a sum of separate gradations, which is the sum of radial and axial gradations for the two-dimensional operation and sum of radial, axial and angular gradations for three-dimensions.

The various results generated are presented in graphical and tabular forms separately for the 2 and 3-dimensions as well as comparatively in some cases. For all cases, the following notation holds:

$$\begin{aligned} C_2H_6 &\equiv A; C_2H_4 \equiv B; C_3H_8 \equiv C; C_3H_6 \equiv \\ D; C_2H_2 &\equiv E; CH_4 \equiv F; C_4H_6 \equiv G; H_2 \equiv H \end{aligned}$$

For the 2-dimensional considerations, Fig. 2 shows the 2-dimensional concentration profile variation with reactor axial length for all reacting specie. As plotted, the concentration of ethane decreased from 0.00107 to 0.00016 kmol/m³ at the reactor exit, while other species rose from zero at the inlet to their respective predicted values as expected. For instance ethane concentration increases from 0 to 0.00091 kmol/m³. The temperature profile variation with reactor axial length is presented

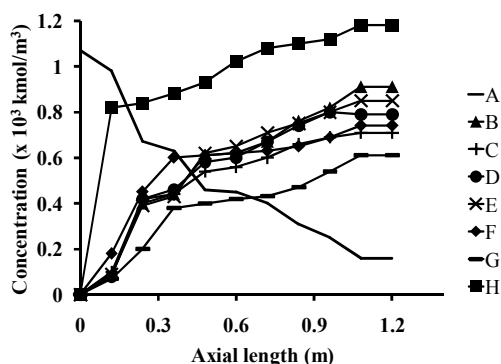


Fig. 2: Concentration profile variation with reactor axial length for all components

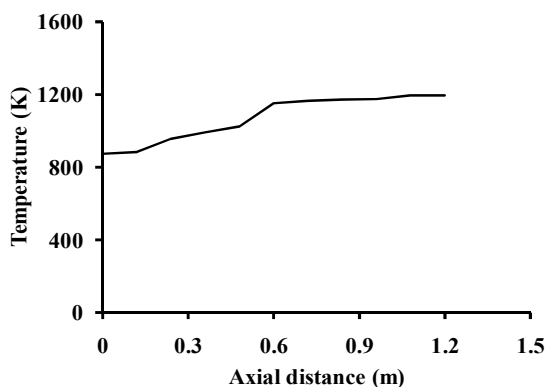


Fig. 3: Temperature profile variation with reactor axial length

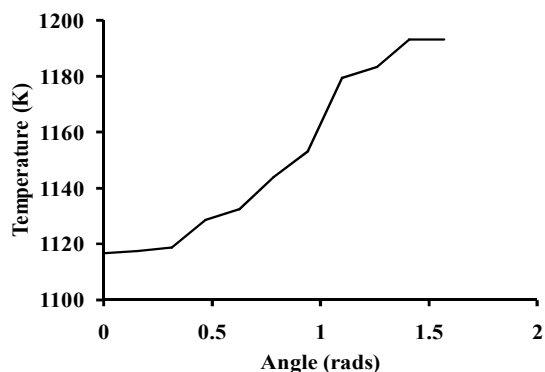


Fig. 4: Angular 3-dimensional variation with temperature at $z = 0.6$ m and $r = 0.002$ m

in Fig. 3. This is seen to rise from about 873.16 to 1193.53 K at the reactor exit.

The 3-dimensional concentration and temperature variations with axial position is almost similar to those of the 2-dimensional profiles, hence the plots are unnecessary. The main target being reported is to really highlight the 3-dimensional contributory effect.

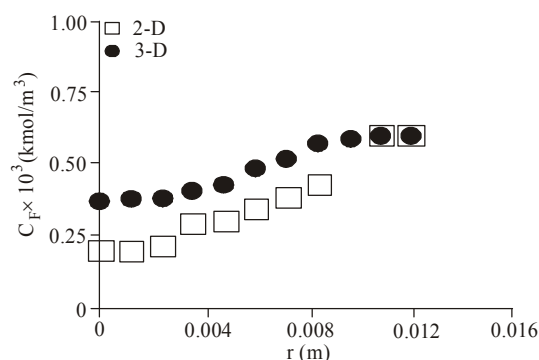


Fig. 5: Radial 2-D and 3-D plots for methane at $z = 0.82$ m

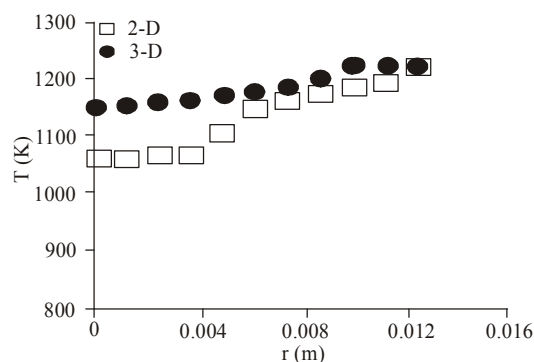


Fig. 6: Radial 2-D and 3-D plots for temperature at $z = 0.82$ m

Table 2 shows the concentration variation with angle at axial length of 0.6 m and radius of 0.002 m, while Fig. 4 shows the angular 3-dimensional variation with temperature at $z = 0.6$ m and $r = 0.002$ m.

The 3-D development presented a more realistic profile by taking into account the limitation on circumferential heating. It corrected this assumption and showed that different diametric segments of the reactor tube exhibit different properties. It also showed that, albeit small, angular variations exist and should be taken into account in the design of tubular thermal cracker tubes. This is pointed out in the concentration variation with radial position plots for methane and temperature as shown in Fig. 5 and 6 respectively. The percentage concentration rise of some parameters for the 2-D and 3-D profiles are also given in Table 2 to 5. It can be deduced that the radial variations are more pronounced than the angular variations for all cases considered. This means that the 3-D profiles is also able to give a smoother change in process variables with variation in process conditions.

The simulated profiles also matched reported experimental data as the conversion of ethane feed is

Table 2: Concentration variation with angle at axial length of 0.6 m and radius of 0.002 m

θ (rad)	Concentration ($\times 10^3$ kmol/m ³)							
	C _A	C _B	C _C	C _D	C _E	C _F	C _G	C _H
0.0000	0.3410	0.7250	0.3640	0.7320	0.7330	0.3630	0.7330	0.7310
0.1570	0.3390	0.7260	0.3650	0.7330	0.7350	0.3640	0.7350	0.7290
0.3140	0.3370	0.7270	0.3670	0.7340	0.7370	0.3650	0.7360	0.7330
0.4710	0.3360	0.7280	0.3690	0.7360	0.7380	0.3680	0.7390	0.7340
0.6280	0.3350	0.7310	0.3710	0.7370	0.7390	0.3720	0.7410	0.7350
0.7850	0.3350	0.7320	0.3720	0.7380	0.7400	0.3740	0.7430	0.7350
0.9420	0.3340	0.7370	0.3740	0.7390	0.7420	0.3750	0.7450	0.7360
1.1000	0.3310	0.7380	0.3760	0.7410	0.7440	0.3770	0.7460	0.7390
1.2600	0.3290	0.7390	0.3770	0.7450	0.7460	0.3790	0.7470	0.7410
1.4100	0.3270	0.7460	0.3790	0.7470	0.7470	0.3810	0.7490	0.7430
1.5700	0.3270	0.7460	0.3790	0.7470	0.7470	0.3810	0.7490	0.7430

Table 3: Two dimensional percentage concentration rise of reacting species from radial distance of 0-0.0125 m at $z = 0.6$ m

Parameter	C _B	C _C	C _D	C _E	C _F	C _G	C _H	T
Increase (%)	2.8154	2.2769	2.8521	2.7795	1.9206	2.8560	2.7643	1.5270

Table 4: Three dimensional percentage concentration rise of reacting species from radial distance of 0-0.0125 m at $z = 0.6$ m and $r = 0.002$ m

Parameter	C _B	C _C	C _D	C _E	C _F	C _G	C _H	T
Increase (%)	0.2098	0.2150	0.2187	0.2379	0.5944	0.1838	0.1274	0.0625

Table 5: Three dimensional percentage concentration rise of reacting species from angular variation of $0-\pi/2$ rad at $z = 0.6$ m and $r = 0.002$ m

Parameter	C _B	C _C	C _D	C _E	C _F	C _G	C _H	T
Increase (%)	0.0290	0.0412	0.0205	0.0191	0.0496	0.0218	0.0164	0.0685

about 85.05% from reactor entrance to exit similar to comparable experimental conditions (Fagley, 1992). Choudhary *et al.* (2006) also obtained 50 to 90% conversion of ethane in a tubular thermal cracker between 1023 to 1173 K.

If the purpose of a design procedure is a general overview of how the tubular thermal cracker operates, then the 2-D model should satisfy this requirement. However, if an in-depth analysis is desired then the 3-D model technique seems preferable.

CONCLUSION

The modelling and simulation of the isothermal tubular thermal cracker for conversion of ethane was carried out with two and three dimensional developments. The simulated reactant and product distribution and temperature profiles are similar to previous observations as observed by Garg *et al.* (2006). It was found that the concentration of all the products increased in directions of increasing temperature while that of ethane reduces in the radial, axial and angular directions.

The results obtained for the 2-D model when compared to those of the 3-D model implied that if angular gradients are ignored, inadequate profiles seem inevitable as axial symmetry is assumed. As observed, even though angular variations seem small, their existence is evident and could be put into consideration when designing a tubular thermal cracker. Furthermore the models presented serves as good predictive tools in

the operation of tubular thermal crackers, which could also be utilized in designing more efficient reactors.

NOMENCLATURE

A	:	Ethane
A_0	:	Frequency factor (conc. ¹⁻ⁿ /s)
B	:	Ethene
C	:	Propane
$C_{j,i}$:	Concentration of species i (discretized form) (kmol/m ³)
C_i	:	Concentration of species i (kmol/m ³)
C_{i0}	:	Concentration of species i at entrance of reactor (kmol/m ³)
C_p	:	Specific heat (J/kg.K)
D	:	Propylene
D_i	:	Diffusivity of species i (m ² /s)
E	:	Ethyne
F	:	Butadiene
G	:	Methane
H	:	Hydrogen
h_r	:	Step length in radial direction
h_θ	:	Step length in angular direction
h_z	:	Step length in axial direction
ΔH_{rxn}	:	Heat of reaction (J/mol)
k_e	:	Effective thermal conductivity (W/m.°C)
k_i	:	Reaction rate constant of reaction i (conc. ¹⁻ⁿ /s)
L	:	Length of the reactor (m)
r	:	Radius (m)
R	:	Pipe radius (m)

r_i : Rate of reaction of specie i (kgmol/m³.s)
 T : Process temperature (K)
 T_0 : Inlet temperature (K)
 T_W : Wall temperature (K)
 U_z : Molar average velocity (m/s)
 χ_A : Conversion of specie A
 Z : Reactor axial dimension

Greek letter:

ρ : Density (kg/m³)

REFERENCES

- Behlolav, Z., P. Zamostny T. and Herink, 2003. *Chem. Eng. Process.*, 42(2003): 461-473.
- Choudhary, V.R., K.C. Mondal and S.A.R. Mulla, 2006. Non-catalytic pyrolysis of ethane to ethylene in the presence of CO₂ with or without limited O₂. *J. Chem. Sci.*, 118(3): 261-267.
- Fagley, J.C., 1992. Simulation of transport in laminar: Tubular reactors and application to ethane pyrolysis. *Ind. Eng. Chem. Res.*, 31: 58-69.
- Froment, F.G. and K.B. Bischoff, 1990. *Chemical Reactor Analysis and Design*. 2nd Edn., John Wiley and Sons, Canada, pp: 400-496.
- Garg, R.K. and V.K. Srivastava, 2001. A Modeling Approach to Thermal Cracking in an Annular Reactor-Quencher. Chemical Engineering Department, Indian Institute of Technology, Delhi.
- Garg, R.K. and V.K. Srivastava, 2006. Modelling and simulation of a non-isothermal tubular cracker. *J. Chem. Eng. Jpn*, 39(10): 1057-1064.
- Garg, R.K., V.V. Krishnan and V.K. Srivastava, 2006. Prediction of concentration and temperature profiles for non-isothermal ethane cracking in a pipe reactor. *Korean J. Chem. Eng.*, 23(4): 531-539.
- Himmeblau, D.M., 1989. *Basic Principles and Calculations in Chemical Engineering*. 5th Edn., Prentice Hall, USA, pp: 18-30.
- Holman, A., O. Olsvick and O.A. Rakstad, 1995. Pyrolysis of natural gas: Chemistry and concepts. *Fuel Process. Technol.*, 42: 249-267.
- Houzelot, J.L. and J. Villiermaux, 1977. Mass transfer in annular cylindrical reactors in laminar flow. *Chem. Eng. Sci.*, 32: 1465-1470.
- Niaei, A., J. Towfighi, S.M. Sadrameli and R. Karimzadeh, 2004. The combined simulation of heat transfer and pyrolysis reactions in industrial cracking furnaces. *Appl. Therm. Eng.*, 24(14-15): 2251-2265.
- Perry, J.H. and C.H. Chilton, 1997. *Chemical Engineers Handbook*. 7th Edn., McGraw Hill Book Co., New York, pp: 50-400.
- Rutherford, A.B., 1989. *Elementary Chemical Reactor Analysis*. John Wiley and Sons, U.S.A., pp: 259-320.
- Sundaram, K.M. and G.F. Froment, 1979. A comparison of simulation models for empty tubular reactors. *Chem. Eng. Sci.*, 34: 117.
- Sundaram, K.M. and G.F. Froment, 1980. Two dimensional model for the simulation of tubular reactors for thermal cracking. *Chem. Eng. Sci.*, 35: 364.
- Walter, J.L., W.W. Bannister, E.T. Moorehouse and R.E. Tapscott, 1988. Anomalous high flammability of low volatility fuels due to anomalously low ignition temperatures. *Am. Chem. Soc. Div. Gas Fuel Chem., Prepr.*, 33(2): 395-402.
- Xu, Q., B. Chen and X. He, 2002. A fast simulation algorithm for industrial cracking furnaces. *Hydrocarb. Process.*, 81: 65.